Estimating the Acid–Base Properties and Electrical Charge of Organic Matter Using Spectrophotometry

Marawit Tesfa, Aline Dia, Fabrice Mahé, Noémie Janot, Rémi Marsac

Estimating the acid-base properties and electrical charge of organic matter using spectrophotometry

Marawit TESFA[1*], Aline DIA[1], Fabrice MAHE[2], Noémie JANOT[3], Rémi MARSAC[1*]

1 Univ. Rennes, CNRS, Géosciences Rennes - UMR 6118, F-35000, Rennes, France

2 Univ. Rennes, CNRS, IRMAR - UMR 6625, F-35000 Rennes, France

3 INRAE Bordeaux Sciences Agro, ISPA - UMR 1391 - 33882 Villenave d'Ornon, France

*Corresponding authors: marawittesfa.research@yahoo.com and remi.marsac@cnrs.fr

Abstract

Spectrophotometric acid-base titration is a simple and powerful technique to evaluate the properties of proton binding sites of natural organic matter (NOM) at environmentally relevant concentrations. However, it is challenging to quantify the chemical charges (Q) carried by NOM at these concentrations. Based on a previous work, which relates the variation of Q with the specific UV-vis differential absorbance ($\Delta A_{\lambda,pH}$) at a given wavelength (λ) and pH of a dissolved NOM sample, the present work proposes a method to investigate any NOM sample. It determines specific features in the absorbance spectra attributed to proton-inert chromophores ($A_{0,\lambda}$), and to the deprotonation processes of carboxylic ($A_{1,\lambda}$) and phenolic groups ($A_{2,\lambda}$). It enables to select sample-specific wavelength (λ_{mid}), where both these functional groups significantly contribute to the variation of absorbance with pH. The linear regression analysis of $A_{\lambda mid,pH}$ vs. Q for various NOM reference samples evidenced that the sample-specific slope (S_{NOM}) and intercept (I_{NOM}) were related to the intrinsic spectroscopic properties of the sample ($A_{0,\lambda mid}$, $A_{1,\lambda mid}$ and $A_{2,\lambda mid}$). This approach can thus be used to approximate the Q values of the NOM samples at environmentally relevant concentrations: a pre-requisite for predicting the fate and behavior of metal ions in natural systems.

Synopsis. This article provides an empirical approach to approximate the charge of natural organic matter at environmentally relevant concentrations using a novel deconvolution method for absorbance spectra.

Keywords: Natural organic matter, acid-base functional groups, proton titration, absorbance spectra

Graphical abstract

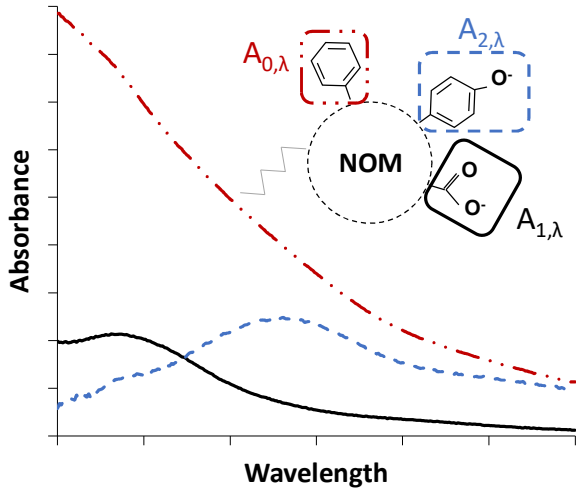

Introduction

Natural organic matter (NOM) is a ubiquitous component in the Critical Zone that profoundly influences the biogeochemical cycles of various contaminants and nutrients, by exerting a strong control on their transport, speciation, (bio)availability and eventually biotoxicity.[1–3] Natural organic matter is known as a major trace cation vector in the environment, as it can bind significant amounts of diverse dissolved metal ions.[4–9] The interaction of NOM with natural and anthropogenic nanoparticles, either organic or inorganic, often increases their colloidal stability,[10–13] therefore enhancing their mobility. Conversely, the binding of NOM to mineral surfaces may affect its chemical stability, reactivity and transport and hence, the biogeochemical cycle of carbon in soils and aquatic systems, as well as that of associated elements and contaminants.[13–19]

The common link between all the above-listed mechanisms is the involvement of NOM functional groups exhibiting acid-base properties.[20–24] These functional groups are generally divided into carboxylic and minor groups often referred to as phenolic groups, which can form complexes with metal ions, in solution or at the (nano)particles' surfaces.[19,20,23,25] Therefore, it is essential to accurately determine the concentration of the NOM acid-base functional groups in natural systems in order to predict the behavior and fate of contaminants with geochemical speciation modeling.[18,21,22,25,26] However, because the carboxylic and phenolic site densities vary broadly with the origin of the NOM, this crucial model input data is rarely available. As a panacea, the generic values proposed by Milne et al.[27] are commonly used,[9,28–30] which might have detrimental consequences on the performance of predictive geochemical models. The most accurate approach to quantify NOM functional groups involves potentiometric acid-base

titration. By direct measurement of the electrical charge carried by humic substances, this titration enables the determination of NOM proton-binding site concentrations, along with their protonation constant and their chemical heterogeneity.[4,23,24,27] Unfortunately, although highly accurate, potentiometric titration cannot be applied to environmental samples, given that the NOM concentrations rarely exceed 100 milligrams of dissolved organic carbon per liter (mgC L^{-1}): such concentrations are too low for optimal electrode measurements requiring several hundreds of mgC L^{-1}.

More recently, the NOM acid-base properties were determined using UV-spectrophotometry, a method requiring lower NOM concentrations similar to natural conditions.[31–35] In addition, this approach is a simple, rapid and low-cost analysis of the NOM acid-base properties. It is based on the observation that the UV-vis absorption of a dissolved NOM sample increases with increasing pH. Differential absorbance ($\Delta A_{\lambda,pH}$) spectra are calculated by the subtraction of a reference absorbance value ($A_{\lambda,pHref}$), usually recorded at low pH (e.g. pH_{ref} = 3), from the absorbance value measured for the same sample at higher pH:

$$\Delta A_{\lambda,pH} = A_{\lambda,pH} - A_{\lambda,pHref} \quad (1)$$

This operation aims to remove the typical featureless absorbance spectra of NOM chromophores exhibiting no acid-base properties and, hence, to identify the small variations in absorbance related to the deprotonation of the NOM functional groups of interest.[31,32,36–38] The differential absorbance spectra of NOM generally show two peaks: a first peak, with a maximum at ~270 nm for which the intensity notably increases between pH 3 and 6 and a second one, with a maximum at 320-380 nm, which appears at pH values above 6. On the basis of their acid-base properties, these peaks can be attributed to the deprotonation processes of the carboxylic and phenolic groups, respectively. By optimizing the parameters of a modified NICA-Donnan model in order to fit the values of $\Delta A_{\lambda,pH}$, it then becomes possible to determine the protonation constants (pK_{a1} and pK_{a2}) of the NOM carboxylic (1) and phenolic (2) groups and their heterogeneity parameters (m_1 and m_2), as well as the specific contribution of the deprotonation process of these groups to the variation of the absorbance ($A_{1,\lambda}$ and $A_{2,\lambda}$).[31,32,35] The choice of wavelength selected is not very important, however it might be preferable to select the value of λ corresponding to the maximum differential absorbance.[32,39]

Although the currently used UV-spectrophotometric acid-base titration approaches provide reliable information on the reactivity of the NOM acid-base functional groups, they do not directly provide charge values from which the concentrations of the carboxylic and phenolic

groups can be estimated. Therefore, other techniques must also be used. To obtain this information, Janot et al. [32] combined potentiometric and spectrophotometric titration of purified Aldrich humic acid (PAHA) to establish a linear relationship between $\Delta A_{\lambda,\mathrm{pH}}$ and the variation of charge (ΔQ). This allowed to investigate the impact of PAHA adsorption and fractionation at the alumina surface on the PAHA acid-base properties.[39] Unfortunately, before now, this relationship has not been tested on different NOM samples, which differ from PAHA in their chemical properties, and thus, might not yet be applicable in environmental conditions.

In the present study, we propose to expand the investigation of the relationship between $\Delta A_{\lambda,pH}$ and ΔQ previously observed by Janot et al.[32] to other NOM samples with various origins and chemical properties. This work attempts to generalize a relationship between $A_{\lambda,pH}$ and Q in order to fully estimate the proton-binding properties of NOM using spectrophotometric data, avoiding the often-impossible collection of potentiometric data. To do so, in this work, recent potentiometric acid-base titration results obtained for seven of the samples provided by the International Humic Substances Society (IHSS) were used.[40] In addition, a novel data treatment of spectrophotometric titrations is proposed to (i) directly deconvolute absorbance $A_{\lambda,pH}$ instead of the differential absorbance $\Delta A_{\lambda,pH}$, to limit potential biases linked to NOM aggregation which might occur at low $\mathrm{pH_{ref}}$,[37,41] and to (ii) take advantage of the complete absorbance dataset collected at λ ranging from 200 to 800 nm or to select the most relevant λ value to derive the NOM-proton binding parameters and NOM charge from the absorbance data.

Materials & Methods

Reagents. All NOM samples used in this study were purchased from the IHSS. Along with their IHSS reference code, there are three samples from Suwannee River: one fulvic acid (FA), one humic acid (HA) and one natural organic matter (NOM) named SRFA (3S101F), SRHA (3S101H) and SRNOM (2R101N), respectively; two samples from Pahokee Peat (PPFA (2S103F) and PPHA (1S103H)); and two HA soil samples: one from Leonardite (LHA, 1S104H) and one from Elliot Soil (ESHA, 4S102H). Data for SRFA were taken from our previous study.[34] Reagents such as HCl, NaOH, NaCl, and the pH-buffers tris(hydroxymethyl)aminomethane (TRIS), 3-(N-morpholino)propanesulfonic acid (MOPS), 2-(N-morpholino)ethanesulfonic acid (MES) and acetic acid (AA) (see Appendix A, Table S1, in the Supplementary Information (SI)) were purchased from Sigma Aldrich. All samples were prepared with ultrapure water provided through a Milli-Q purification system.

Sample preparation. A 250 mL NOM mother solution (1 g L^{-1}) was prepared by dissolving 25 mg of NOM powder using NaOH (0.1 mol L^{-1}) in ultrapure water. Complete dissolution was ensured by maintaining the pH of the NOM solution at around 9 upon the addition of NaOH. All pH measurements were performed with a HANNA, HI5221 pH meter. The pH of the NOM mother solution was monitored for 24 hours, with adjustments performed at 3, 6 and 12 hours after the start of the NOM dissolution process. The NOM mother solution was left to mix on a shaking table in-between these pH adjustments. Subsequently, the dissolved organic carbon concentration (DOC) was determined through a Shimadzu TOC-L analyzer. The NOM samples destined to be analyzed by spectrophotometric acid-base titration were prepared by diluting the mother solution to a carbon concentration of 25 mgC L^{-1}, and by adjusting their ionic strength (IS) to 0.01 mol L^{-1}, with NaCl.

The preparation of the buffer solutions followed the protocol described in a previous article.[34] Briefly, buffer salt was dispersed in a total of 50 mL volume of ultrapure water at final concentration of 1 mol L^{-1}. The pH of the buffer solution was adjusted to match the pKa value of the buffer salt, or values within pKa - 1 < pH < pKa + 1 with acid (HCl, 1, 0.1 mol L^{-1}) or base (NaOH, 1, 0.1 mol L^{-1}) addition. A total of 11 buffer solutions, with pH values ranging from 3.8 to 9, were prepared with four initial buffer salts TRIS, MOPS, MES and AA (Appendix A, Table S1 in the SI).

Spectrophotometric acid-base titration. The spectrophotometric acid-base titration was also carried out as described in a previous study.[34] Each of the studied NOM samples was divided into 13 aliquots of 4 mL (25 mgC L^{-1} and 0.01 mol L^{-1} NaCl). The pH of the 11 aliquots of the NOM solution, ranging from pH 3.8 to 9, was fixed using the corresponding buffer, with a final buffer concentration of 10^{-3} mol L^{-1}. The pH of the two remaining aliquots was adjusted to pH 3 and 3.4 using HCl. The pH was monitored for 15 minutes to ensure it was stable before proceeding to the absorbance measurement. Subsequently, the raw UV-vis absorbance of each aliquot was recorded for wavelengths (λ) between 200-800 nm, using a UV-vis Shimadzu UV2600 spectrophotometer and a 1-cm-wide quartz cuvette. In this study, the raw absorbance ($A_{\lambda,pH,raw}$) in this study was normalized by the DOC data and by the optical pathlength, in order to determine the specific UV absorbance spectra, as detailed in the following equation (Eq. 2)

$$A_{\lambda,pH} = \frac{1}{l_{cell}} \times \frac{A_{\lambda,pH,raw}}{DOC} \qquad (2)$$

The specific UV absorbance spectra, here denoted "$A_{\lambda,pH}$" (in cm^{-1} gC^{-1} L) for simplicity, is commonly referred to as "SUVA" in the literature. The specific absorbance spectra, above 540 nm, contain little information and, as demonstrated in a previous study,[34] the absorbance of the pure buffer solutions is limited to $\lambda < 240$ nm. Consequently, all data treatments were conducted within a λ range of 240 nm – 540 nm.

Results & Discussion

Spectrophotometric titration results. The specific absorbance spectra (A vs. λ) were measured at different pH values for each IHSS sample (Appendix B, Figure S1 in the SI). The resulting spectra are typical of NOM, i.e., featureless decreasing specific absorbance spectra with increasing wavelength.[31,32,36,37] The specific absorbance also increases with increasing pH. This effect can be observed by inspecting the variation of the specific absorbance spectra at a given wavelength ($\Delta A_{\lambda,pH}$) as a function of pH with respect to a reference spectrum.[31,32,37] The corresponding $\Delta A_{\lambda,pH}$ values, calculated using equation 1 and the specific absorbance spectrum recorded at pH = 3 as a reference, are plotted in Figure 1 for the seven IHSS samples investigated. The present data are in excellent agreement with previous acid-base spectrophotometric titrations of the IHSS samples.[31–33] All samples display two characteristic peaks of the deprotonation process of the carboxylic (with a maximal absorbance at ~270 nm) and phenolic groups (with a maximal absorbance at ~350 nm), the intensity of which increases with increasing pH over two distinct pH-ranges. Note that, if each type of acid-base functional groups exhibits a maximal absorbance values, they can absorb photons on large λ-ranges because a large diversity of chromophores is included in each group. The intensity of the peak at 270 nm increases between approximately pH 3 and 7, whereas the peak at 350 nm only appears at pH values above 6. The variation range of $\Delta A_{\lambda,pH}$ as a function of pH is different depending on the sample. For instance, compared to humic samples (SRFA vs. SRHA and PPFA vs. PPFA), fulvic samples seem to have lower variation in the absorbance range. Additionally, the specific absorbance intensity of the carboxylic and phenolic deprotonation processes varies depending on the origin of the sample. The samples from Suwannee River (SRFA, SRHA and SRNOM) display a more intense $\Delta A_{\lambda,pH}$ peak around 350 nm compared to the peak at 270 nm. This trend is inverted in the other samples where the 270 nm peak is always more intense than the peak at ~350 nm. For this reason, it is crucial to consider both carboxylic and phenolic deprotonation processes in the procedure for specific absorbance deconvolution.

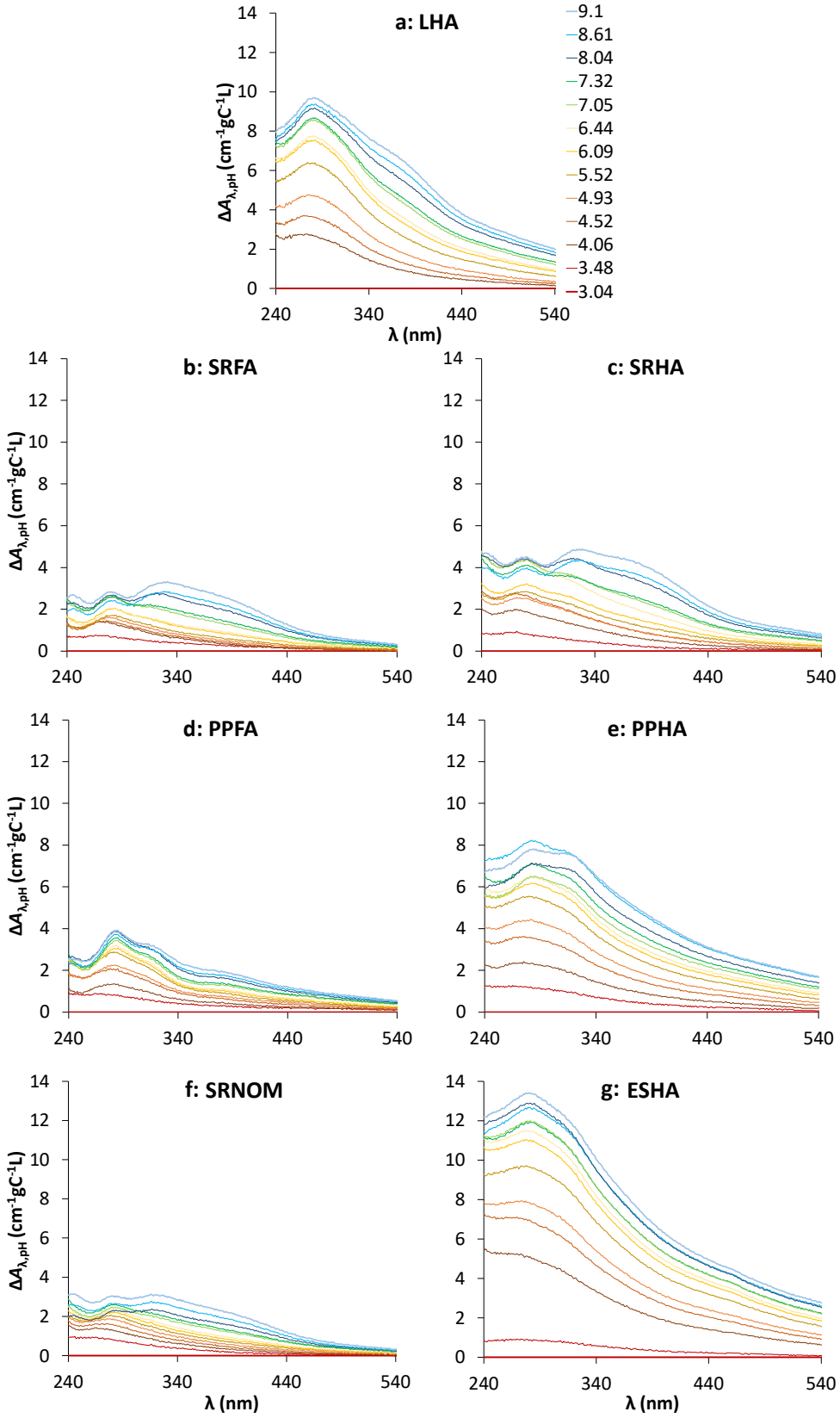

191

192 **Figure 1**. Differential specific absorbance spectra ($\Delta A_{\lambda,pH}$ in $cm^{-1}gC^{-1}L$) of (a) LHA, (b) SRFA[34], (c)
193 SRHA, (d) PPFA, (e) PPHA, (f) SRNOM and (g) ESHA derived from the absolute specific
194 absorbance spectra ($A_{\lambda,pH}$). The spectra were recorded at different pH values, from 3.04 to 9.10 (the
195 same colors are used in all figures).

196

Deconvolution of absolute specific absorbance spectra. The approach described above outlines the methods used so far in previous studies to characterize NOM through UV-vis spectroscopy.[31–33] This approach might present a potential bias related to NOM aggregation at low pH,[37,41] which may arise when using the data collected at pH 3 as a reference for the calculation of $\Delta A_{\lambda,\mathrm{pH}}$. In addition, the subtraction process removes part of the information contained in the data because, even at pH 3, a significant fraction of the carboxylic groups might be deprotonated.[24,27,40] Lastly, when further interpreting the data, the focus on a single wavelength discards the information throughout the rest of the data at different λ. As an alternative approach used in the present work, the deconvolution of the specific absorbance spectra was inspired from previous studies but carried out on the specific absorbance spectra throughout the entire wavelength range (240 nm – 540 nm). This operation was conducted using the Matlab™ software, in which a model (Eq. 3) describing the specific absorbance spectra has been implemented:

$$A_{\lambda,pH} = A_{0,\lambda} + A_{1,\lambda} \times f_{1,pH} + A_{2,\lambda} \times f_{2,pH} \qquad (3)$$

The mathematical development leading to equation 3 is given in Appendix C in the SI. With equation 3, we hypothesize that the experimentally measured specific absorbance ($A_{\lambda,pH}$) is a linear combination of three components ($A_{0,\lambda}$, $A_{1,\lambda}$ and $A_{2,\lambda}$), two of which ($A_{1,\lambda}$ and $A_{2,\lambda}$) are associated with their pH-dependent coefficients ($f_{i,pH}$). The component $A_{0,\lambda}$ mainly represents the proton-inert chromophores within the investigated pH range. According to the calculations, $A_{0,\lambda}$ also includes the specific absorbance of the proton-reactive chromophores under their protonated form (Appendix C, Eq. S5 in the SI). The $A_{1,\lambda}$ and $A_{2,\lambda}$ components are attributed to the deprotonation process of the carboxylic and phenolic groups, respectively. Thus, both $A_{1,\lambda}$ and $A_{2,\lambda}$ represent the difference in specific absorbance between the deprotonated and protonated species of the acid-base functional groups. The coefficients $f_{1,pH}$ and $f_{2,pH}$ are the fractions of deprotonated chromophores at the corresponding pH. Consequently, $A_{0,\lambda}$ is not associated with a pH-dependent coefficient $f_{i,pH}$. All of the parameters ($A_{0,\lambda}$, $A_{1,\lambda}$, $f_{1,pH}$, $A_{2,\lambda}$, $f_{2,pH}$) were optimized to best fit the experimental $A_{\lambda,\mathrm{pH}}$ values using an iterative optimization method. However, the optimization problem used to estimate the parameters of Eq.3 has multiple solutions but a reasonable *a priori* estimation of the values of the parameters could be obtained on the basis of chemical constraints. The local convergence of the optimization algorithm was used to improve these starting values. The values of $f_{1,pH}$ and $f_{2,pH}$ were constrained to (i) vary

from 0 to 1 (as they represent fractions) and to (ii) increase with rising pH. These constraints facilitated the convergence of $f_{1,pH}$ and $f_{2,pH}$ to chemically realistic values. A detailed explanation of the optimization process, including the choice of starting values, is given in the SI (Appendix D in the SI). Figure 2 shows the results of the deconvolution process for all IHSS samples. Based on the $\Delta A_{\lambda,\mathrm{pH}}$ calculations carried out in the previous section, the variation of specific absorbance related to the increase in pH (i.e. the deprotonation process) represents less than 1% of the total variation found in the $A_{\lambda,pH}$ vs. λ curve. As a consequence, the $A_{0,\lambda}$ for all seven IHSS samples (Figure 2a) is similar to their own raw specific absorbance spectra (Appendix B, Figure S1 in SI). The characteristic components of the carboxylic and phenolic groups ($A_{1,\lambda}$ and $A_{2,\lambda}$) display a peak shape with a maximum at $\lambda \approx 270$ nm and λ ranging from 320 to 370 nm, in agreement with previous investigations involving a differential absorbance analysis.[31,33] The fractions of deprotonated carboxylic ($f_{1,pH}$) and phenolic ($f_{2,pH}$) groups as a function of pH for all samples are depicted in Figure S2 (Appendix E in the SI). Using the Langmuir-Freundlich equation (Eq. 4) and a least-square fitting procedure, the $f_{1,pH}$ and $f_{2,pH}$ vs. pH curves obtained can be further processed to determine the apparent protonation constants (K_1 and K_2) and heterogeneity parameters (m_1 and m_2) of the proton binding sites:

$$f_{\mathrm{i,pH}} = \frac{1}{1+(K_i\,[H^+])^{m_i}} \qquad (4)$$

These apparent protonation constants and heterogeneity parameters are detailed in Table S2 (Appendix F in the SI). The values calculated for the carboxylic and phenolic groups are generally in line with those found in the literature, i.e., log K_1 ranging from 3.26 to 4.10, log K_2 ranging from 9.66 to 10.07,[24,42] and the associated heterogeneity parameter with average values of 0.45 for m_1 and 0.20 for m_2.[24]

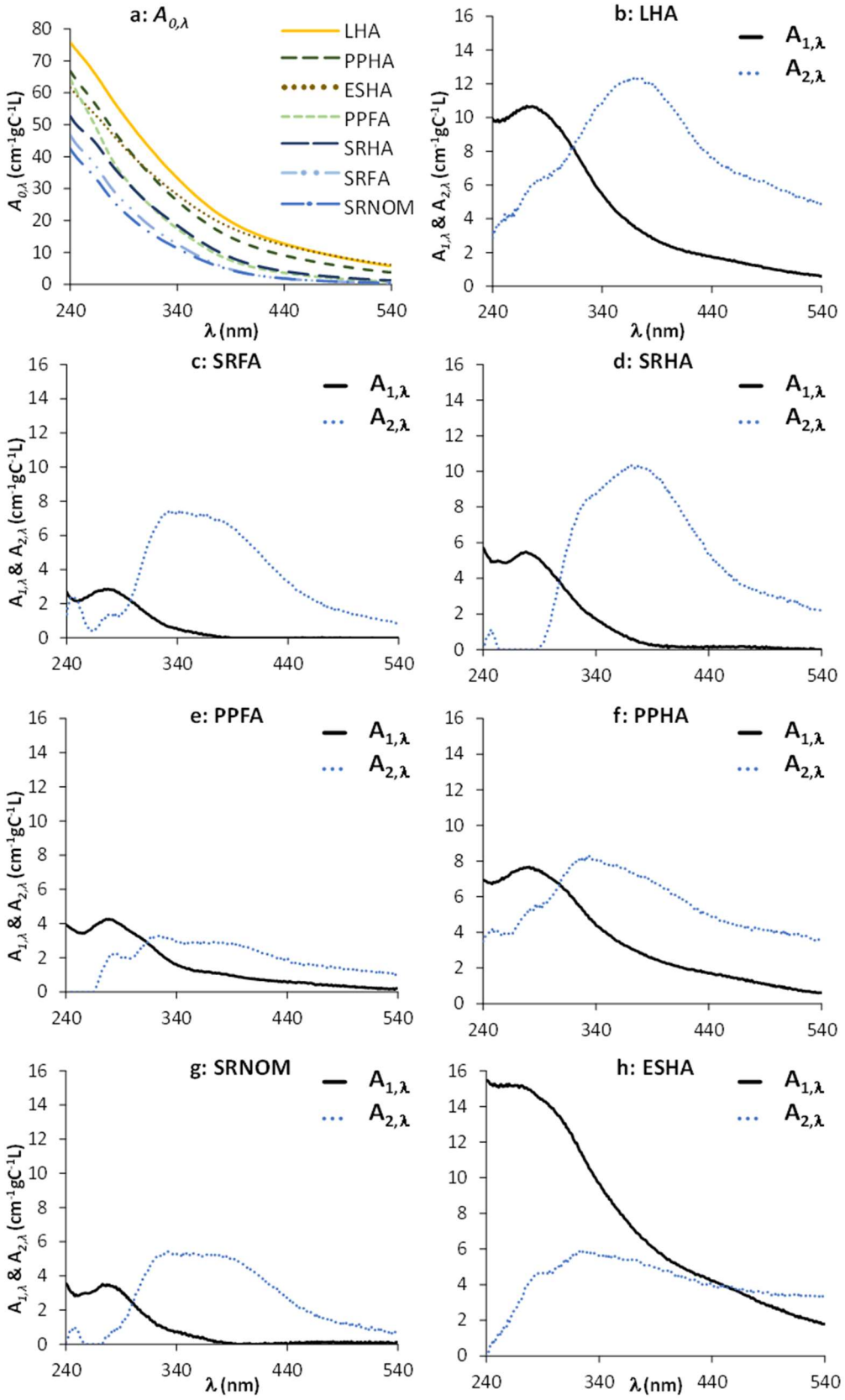

Figure 2. Results of the deconvolution of the acid-base spectrophotometric titration data with equation 3: (a) component $A_{0,\lambda}$ for all samples, $A_{1,\lambda}$ and $A_{2,\lambda}$ components for (b) LHA, (c) SRFA, (d) SRHA, (e) PPFA, (f) PPHA, (g) SRNOM and (h) ESHA.

Relationship between charge and specific absorbance.

As mentioned in the introduction section, it is a major challenge to measure the concentration of the acid-base functional groups in NOM at environmentally-relevant concentrations.[32] Although spectrophotometric methods do provide valuable quantitative information with respect to the acid-base properties of the NOM functional groups, they cannot be used to determine the electrical charge of NOM, from which the functional group density can be deduced. This requires additional measurements such as potentiometric titrations or other spectroscopic techniques (e.g. Infra-Red (IF), Nuclear Magnetic Resonance (NMR)).[24,43] A linear relationship between the differential specific absorbance $\Delta A_{\lambda,\mathrm{pH}}$ and the differential charge ΔQ of PAHA was determined by Janot et al.,[32] which allowed subsequent investigations of the PAHA acid-base properties after its fractionation on the surface of aluminum oxide at environmentally relevant NOM concentrations.[39] However, this relationship was specific to PAHA and it might not be possible to extrapolate it to other NOM with different spectroscopic characteristics as shown above (Figures 1 and 2). Since the seven IHSS samples analyzed in the present study were previously titrated by potentiometry,[40] the relevance of such a relationship between the specific absorbance and the charge is tested for various NOM samples. Setting up a link between $A_{\lambda,pH}$ and Q requires the selection of a representative wavelength. However, the values of $A_{270,\mathrm{pH}}$ [32] or $A_{360,\mathrm{pH}}$ [31] selected in the literature are not suitable for the entire set of samples studied in the present work. Close inspection of the specific absorbance spectra of the carboxylic and phenolic groups for all the presently investigated samples (Figure 2) shows that these functional groups can be almost spectroscopically silent at certain λ ranges. Specifically, $A_{2,\lambda}$ is very low for $\lambda < 300$ nm and $A_{1,\lambda}$ is very low for $\lambda > 320$ nm for SRFA, SRHA, SRNOM and PPFA. As a solution, we propose to determine and use a sample specific λ, at which both carboxylic and phenolic deprotonation processes significantly contribute to the UV-vis absorption. For this purpose, the λ value at the mid-section (λ_{mid}) of the peak of both carboxylic and phenolic specific absorbance spectra was chosen and is listed in Table S3 (Appendix G in the SI) for each NOM sample. A schematic representation of the method used to select the λ_{mid} is shown with an example in Figure S3 (Appendix H in the SI). Typically, the λ_{mid} ranges from 291 to 330 nm (Appendix G in the SI). The specific absorbance at the selected λ_{mid} ($A_{\lambda\mathrm{mid}}$) is represented as a function of the measured Q extracted from a previous work[40] in Figure 3. Note that the Q in this present study was considered in mol gC^{-1} unlike the previous study[40] in which Q was measured in mol kg_{NOM}^{-1}. Details of the unit conversion are given in equation S12 (Appendix I in the SI). Figure 3 shows $A_{\lambda\mathrm{mid}}$ for all seven of the studied IHSS

samples as a function of Q and displays a linear relationship between $A_{\lambda mid.}$ and Q for each sample, which is in agreement with a previous work on PAHA.[32] It is possible to discern three clusters of samples: a first one containing ESHA, LHA and PPHA with high $A_{\lambda mid}$ and low Q values, a second one assembling SRHA, SRFA and SRNOM with low $A_{\lambda mid}$ and low Q values and, finally, a third cluster containing PPFA only, with intermediate $A_{\lambda mid}$ values and the highest Q values. The separation between the humic and fulvic samples is in line with the UV spectroscopy indicators, such as A_{250}/A_{365} (Figure S4, Appendix J in the SI),[44] which are often considered as an indicator of the NOM molecular weight (M_w). The same separation can also be observed when considering the aromaticity of the IHSS samples determined by NMR.[43] Additionally, M_w and the particle radius (r_p) determined in previous studies by using Soft Poisson Boltzmann-based titration (SPBT) formalism were examined.[40] A first clustering between the humic and fulvic samples was observed, in addition to a clustering between the soil samples (with $1.71 < r_p < 3.67$ nm; $3.64 < M_w < 11.10$ kg mol^{-1}) and water samples (with $0.8 < r_p < 1.8$ nm and $1.14 < M_w < 4.02$ kg mol^{-1}). These observations are in agreement with other studies that associated samples with higher weight, size and aromaticity content with plant-sourced terrestrial refractory NOM, as opposed to lighter, smaller and less aromatic NOM, which are often linked to labile water or bacterial sourced NOM.[40,45,46]

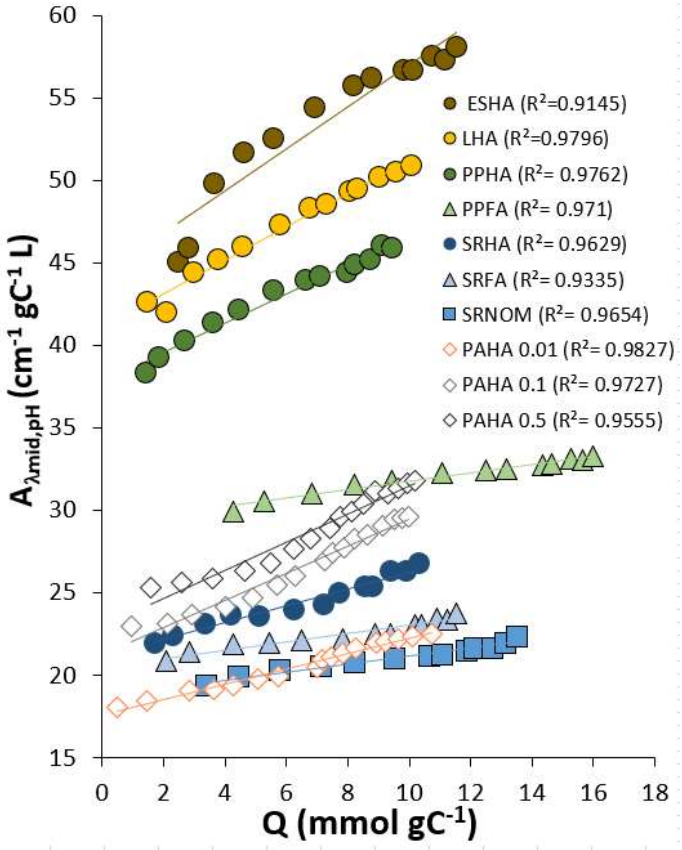

Figure 3. Specific absorbance ($A_{\lambda mid}$ in cm^{-1} gC^{-1} L) at λ_{mid}, as a function of the charge (Q in mmol gC^{-1}) for the seven IHSS samples. Charge values are from Tesfa et al.,[40] solid symbols represent the experimental measurements and corresponding lines represent linear regressions (R^2 in brackets). Data for PAHA were derived from Janot et al.[32]. The slope and intercept values of each linear regression are detailed in Table S4 (Appendix K in the SI).

Each of the established relationships between $A_{\lambda mid}$ and Q exhibits a slope (S_{NOM}) and intercept (I_{NOM}) specific to the corresponding NOM sample, which consequently cannot be extrapolated to other NOM samples:

$$A_{\lambda mid} = I_{NOM} + Q \times S_{NOM} \qquad (5)$$

However, it is proposed here to estimate S_{NOM} and I_{NOM} for any NOM using its UV-vis optical properties. In fact, I_{NOM} can easily be calculated using a combination of equations 3 and 4, and through a comparison with equation 5. In extreme acidic conditions (pH $\rightarrow -\infty$), Q, f_1 and f_2 tend to 0 because all acid-base groups are fully protonated. As a result, $A_{\lambda mid} \rightarrow A_{0,\lambda mid}$ (Eq. 3) and $A_{\lambda mid} \rightarrow I_{NOM}$ (Eq. 5). Thus, $A_{0,\lambda mid}$ can be approximated to I_{NOM}, which is verified with Figure 4a, where I_{NOMS} vs. $A_{0,\lambda mid}$ displays a linear relationship (R^2 = 0.9988) with a slope approximatively equal to 1, and a negligible intercept value if compared to $A_{0,\lambda mid}$ or I_{NOM}. To provide an estimation of S_{NOM}, we hypothesized it to be related to the sum $A_{1,\lambda mid} + A_{2,\lambda mid}$ as described in equation 6, because these parameters concomitantly control the variation of the specific absorbance with pH (Eq. 3).

$$S_{NOM} = S_b + S_a \times (A_{1,\lambda mid} + A_{2,\lambda mid}) \qquad (6)$$

In equation 6, S_a represents the slope and S_b represents the intercept of a linear relationship between S_{NOM} and $A_{1,\lambda mid} + A_{2,\lambda mid}$. Accordingly, Figure 4b exhibits aligned values of S_{NOM} vs. $A_{1,\lambda mid} + A_{2,\lambda mid}$ for all samples, thereby establishing a linear relationship between these parameters (R^2 = 0.9858). Consequently, considering the specific parameters of equation 3 (i.e. $A_{0,\lambda}$, $A_{1,\lambda}$ and $A_{2,\lambda}$) and the carefully selected λ_{mid} might allow to approximate Q for unknown NOM samples using only absorbance data.

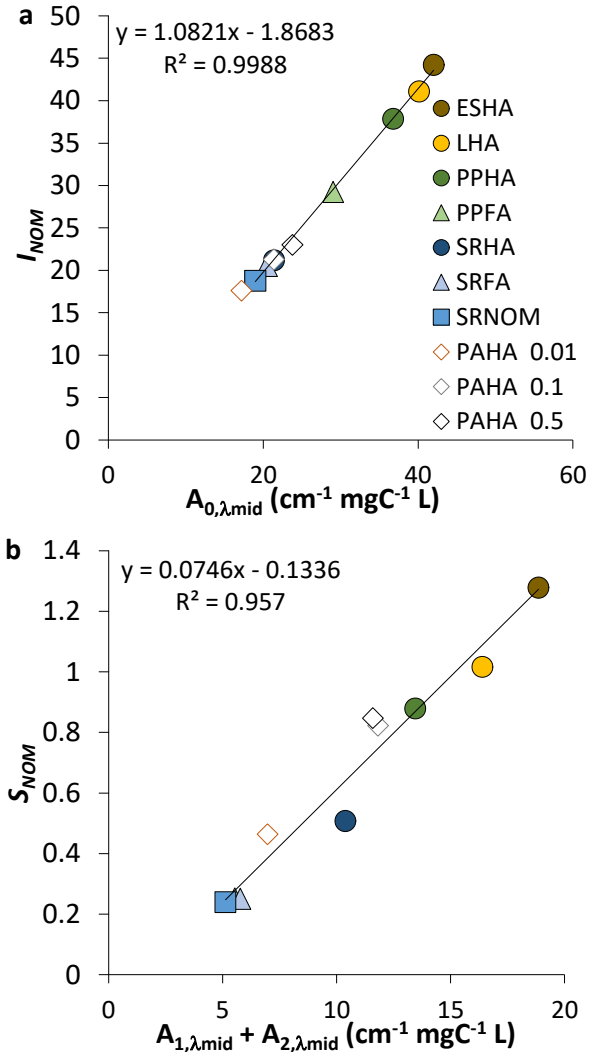

Figure 4. (a) Intercept I_{NOM} and (b) slope S_{NOM} of linear regression between $A_{\lambda mid}$ and Q (equation 5) as a function of $A_{0,\lambda mid}$ and $A_{1,\lambda mid} + A_{2,\lambda mid}$, respectively for all IHSS samples (SRFA, SRHA, SRNOM, PPFA, PPHA, LHA and ESHA), as well as the literature data (PAHA 0.01-0.5; values refer to the ionic strength;[32]), for comparison. Linear regressions do not take the PAHA data into account.

Data from the literature on PAHA[32] were used to corroborate the above-proposed approach using an independent dataset. Because PAHA was titrated by both spectrophotometric and potentiometric acid-base titration data at three different background electrolyte concentrations (0.01, 0.1 and 0.5 mol L^{-1} in $NaClO_4$), the method described here could be tested on a larger range of physico-chemical conditions than the concentration used to establish the method (0.01 mol L^{-1} of NaCl). Hereafter, the three PAHA samples will be referred to as "PAHA 0.01", "PAHA 0.1" and "PAHA 0.5" according to their respective background electrolyte concentrations. As described above for the seven IHSS samples studied here, the three PAHA specific absorbance datasets were deconvoluted using equation 3. After a close inspection of their $A_{1,\lambda mid}$ and $A_{2,\lambda mid}$ values (Figure 5), a λ_{mid} value for each $NaClO_4$ concentration was selected (Appendix G, Table S3 in the SI). Using the potentiometric titration, data from Janot

et al.,[32] $A_{\lambda mid}$ were plotted as a function of Q in Figure 3 and specific I_{PAHA} and S_{PAHA} were extracted and plotted in Figures 4a and 4b, respectively. The three PAHA samples are in very good agreement with the linear relationship established using the seven different IHSS samples, showing an increase in both I_{NOM} and S_{NOM} with increasing electrolyte concentration. The background electrolyte concentration affects proton−NOM binding and, hence, Q as it impacts the electrostatic contribution to the overall interaction between HS and protons.[40] This was previously shown to affect NOM absorbance.[38] Furthermore, ionic strength has more impact on absorbance than on charge measurement. This can be explained by the aggregation of NOM molecules at higher ionic strength, due to charge screening, increasing the interactions between chromophores.[32] Thus, for a same sample, I_{NOM} and S_{NOM} values increase with ionic strength, which is accompanied by an increase in $A_{0,\lambda mid}$ and $A_{1,\lambda mid} + A_{2,\lambda mid}$, respectively. The consistency between the observations made on an independent sample in various ionic strength conditions and on our reference samples validates the approach developed here.

As such, we propose a condensed empirical equation enabling the estimation of Q directly from the specific absorbance data. This empirical equation combines equation 3 with the individual equations relating I_{NOM} *to* $A_{0,\lambda mid}$ ($I_{NOM} \approx A_{0,\lambda mid}$) and linearly relating S_{NOM} to $A_{1,\lambda mid} + A_{2,\lambda mid}$ (Figure 4; eq. 6).

$$Q_{pH} = \frac{A_{\lambda mid,pH} - A_{0,\lambda mid}}{(A_{1,\lambda mid} + A_{2,\lambda mid})S_a + S_b} \qquad (7)$$

By using a least-square fitting procedure, and all the available data in the present work for the IHSS and PAHA samples, we estimated $S_a = 0.089 \pm 0.003$ and $S_b = -0.228 \pm 0.016$ (root-mean-square error, RMSE = 1.29). The assumption of a linear relationship instead of equality between $A_{0,\lambda mid}$ and I_{NOM} was not statistically justified because the decrease in RMSE associated with the optimization of two additional parameters was very small (RMSE = 1.30). The accuracy of the present approach to predict Q is shown in Figure S5 (Appendix L in the SI), where 86% of the experimentally determined values can be calculated (Q_{calc}) within an error range of ± 2 mol kgC^{-1}. Table S5 (Appendix M in the SI), shows the RMSE values for the individual datasets, and demonstrates that the largest error is attributed to SRHA and PAHA 0.01 (RMSE = 2.24 and 2.38, respectively), whereas, for the other NOM samples, 0.48 (PAHA 0.1) ≤ RMSE ≤ 1.13 (ESHA).

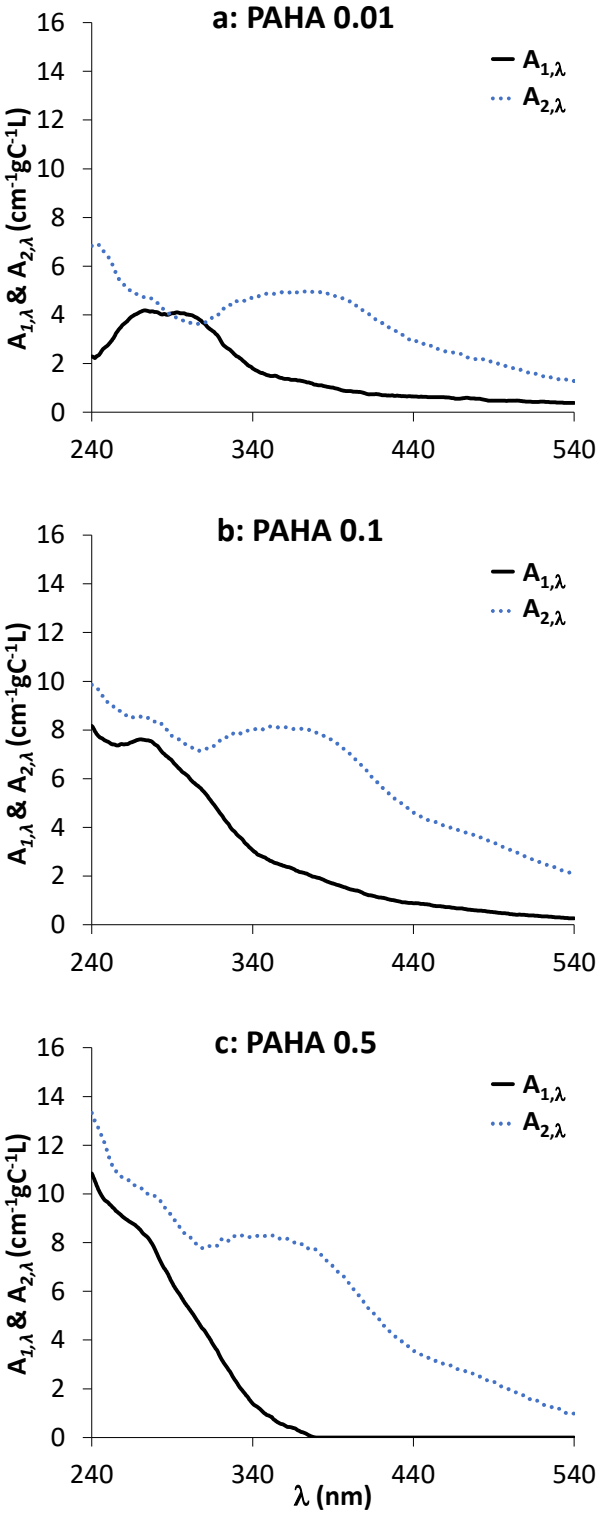

Figure 5. Results of the deconvolution of the acid-base spectrophotometric titration data with equation 3 for the PAHA samples in (a) 0.01, (b) 0.1 and (c) 0.5 M $NaClO_4$.

Environmental implications

Although many important mechanisms involve NOM acid-base functional groups, it is difficult to quantify them in natural samples, especially since it is still a major challenge to determine the NOM charge at environmentally relevant concentrations. To overcome this, we developed, in the present study, a novel UV-vis spectrophotometric method based on a previously established relationship between the ΔA and ΔQ of a NOM sample (PAHA).[32] By extending this finding to various NOM samples, using a recently collected potentiometric titration dataset,[40] it was possible to provide an empirical approach to estimate the charge values of NOM samples using UV-vis absorption data only. The parameters defining the linear relationship between A and Q, i.e. I_{NOM} and S_{NOM}, were themselves linearly related to the proton inert chromophores $A_{0,\lambda mid}$ and to the sum of both proton sensitive chromophores $A_{1,\lambda mid}$ and $A_{2,\lambda mid}$, respectively. The advantage of the empirical approach proposed here to estimate Q is that it (i) does not require to perform a potentiometric acid-base titration, (ii) is based on sample-specific spectra parameters ($A_{0,\lambda mid}$ $A_{1,\lambda mid}$ and $A_{2,\lambda mid}$) and (iii) is also suitable at different background electrolyte concentrations (in $NaClO_4$) compared to the studied concentrations. Because spectroscopy is suitable for NOM sample characterization in terms of their environmental concentration, the novel spectrophotometric deconvolution method developed in the present study, and sample specific empirical spectra analysis could be used to approximate the Q of unknown natural samples and subsequently estimate their carboxylic and phenolic functional groups' concentrations. However, in contrast to Na^+, other cations such as Cu^{2+} or Al^{3+} can bind to NOM and affect the absorbance signal.[47] The present approach might be applicable to natural samples containing cations other than monovalent ones if the interferences on the absorbance spectra they generate remain insignificant. Otherwise, it might be necessary to remove these cations from the sample using a simple purification procedure.

The present approach further allows the estimation of the NOM charge in various aquatic systems, which is critical to understanding the role of NOM in environmental studies. Natural organic matter can be a nanoparticle stabilizing agent, a contaminant vector or a reaction catalyzer. Understanding and predicting the geochemical behavior and transport of aquatic NOM thus requires taking its charge into account, because the charge predominantly controls its interaction with other organic or inorganic particles. Therefore, the present work provides important keys for understanding and predicting the biogeochemical cycle of NOM and its associated elements.

Acknowledgments

This work was supported by the C-FACTOR project funded by ANR (project number ANR-18-CE01-0008; coordinator: R. Marsac). Through the support of the GeOHeLiS analytical platform of Rennes University, this publication is also supported by the European Union through the European Regional Development Fund (FEDER), the French ministry of Higher Education and Research, the French Region of Brittany and Rennes Metropole. Lastly, Dr. S. Mullin is acknowledged for post-editing the English content.

Supporting Information

The supporting information section contains 11 pages, 12 equations, 7 references, 5 tables and 5 figures. It is organized as follows:

Appendix A: Table S1. Characteristics of the buffer salts used to prepare the buffer solutions

Appendix B: Figure S1. Specific absorbance spectra and the corresponding deconvoluted A_0 component.

Appendix C: Mathematical development for equation 3

Appendix D: Script details on the optimization method and constraints used on the estimated parameters for the description of the NOM specific absorbance spectra

Appendix E: Figure S2. Deconvolution results of the deprotonated fractions of the carboxylic and phenolic sites for all seven IHSS samples

Appendix F: Table S2. Apparent protonation constants (log K_1 and log K_2) and heterogeneity parameters (m_1 and m_2) of the carboxylic and phenolic groups, respectively

Appendix G: Table S3. Middle wavelength (λ_{mid}) corresponding to the mid-section between both maxima of the specific spectra for the carboxylic and phenolic groups

Appendix H: Figure S3. Example of how $A_{1,\lambda mid}$ and $A_{2,\lambda mid}$ are selected, shown in two steps

Appendix I: Equation S12 to convert Q from mol kgNOM^{-1} to mol gC^{-1}

Appendix J: Figure S4. Comparison of A_{250}/A_{365} for the IHSS samples

Appendix K: Table S4. Slope (S_{NOM}) and intercept (I_{NOM}) of the linear regression established between specific absorbance and charge

Appendix L: Figure S5. Calculated Q (Q_{cal}) vs. experimental Q (Q_{exp})

Appendix M: Table S5. RMSE values for each NOM dataset

References

(1) Lachaux, N.; Catrouillet, C.; Marsac, R.; Poirier, L.; Pain-Devin, S.; Gross, E. M.; Giamberini, L. Implications of Speciation on Rare Earth Element Toxicity: A Focus on Organic Matter Influence in Daphnia Magna Standard Test. *Environ. Pollut.* **2022**, *307*, 119554. https://doi.org/10.1016/j.envpol.2022.119554.

(2) McCarthy, J. F. Bioavailability and Toxicity of Metals and Hydrophobic Organic Contaminants. In *Aquatic Humic Substances*; Suffet, I. H., MacCarthy, P., Eds.; Advances in Chemistry; American Chemical Society: Washington, DC, 1988; Vol. 219, pp 263–277. https://doi.org/10.1021/ba-1988-0219.ch018.

(3) Peng, C.; Sundman, A.; Bryce, C.; Catrouillet, C.; Borch, T.; Kappler, A. Oxidation of Fe(II)–Organic Matter Complexes in the Presence of the Mixotrophic Nitrate-Reducing Fe(II)-Oxidizing Bacterium Acidovorax Sp. BoFeN1. *Environ. Sci. Technol.* **2018**, *52* (10), 5753–5763. https://doi.org/10.1021/acs.est.8b00953.

(4) Benedetti, M. F.; Milne, C. J.; Kinniburgh, D. G.; Van Riemsdijk, W. H.; Koopal, L. K. Metal Ion Binding to Humic Substances: Application of the Non-Ideal Competitive Adsorption Model. *Environ. Sci. Technol.* **1995**, *29* (2), 446–457. https://doi.org/10.1021/es00002a022.

(5) Catrouillet, C.; Davranche, M.; Dia, A.; Bouhnik-Le Coz, M.; Marsac, R.; Pourret, O.; Gruau, G. Geochemical Modeling of Fe(II) Binding to Humic and Fulvic Acids. *Chem. Geol.* **2014**, *372*, 109–118. https://doi.org/10.1016/j.chemgeo.2014.02.019.

(6) Hiemstra, T.; van Riemsdijk, W. H. Biogeochemical Speciation of Fe in Ocean Water. *Mar. Chem.* **2006**, *102* (3), 181–197. https://doi.org/10.1016/j.marchem.2006.03.008.

(7) Pokrovsky, O. S.; Schott, J.; Dupré, B. Trace Element Fractionation and Transport in Boreal Rivers and Soil Porewaters of Permafrost-Dominated Basaltic Terrain in Central Siberia. *Geochim. Cosmochim. Acta* **2006**, *70* (13), 3239–3260. https://doi.org/10.1016/j.gca.2006.04.008.

(8) Tang, J.; Johannesson, K. H. Speciation of Rare Earth Elements in Natural Terrestrial Waters: Assessing the Role of Dissolved Organic Matter from the Modeling Approach. *Geochim. Cosmochim. Acta* **2003**, *67* (13), 2321–2339. https://doi.org/10.1016/S0016-7037(02)01413-8.

(9) Tipping, E.; Rey-Castro, C.; Bryan, S. E.; Hamilton-Taylor, J. Al(III) and Fe(III) Binding by Humic Substances in Freshwaters, and Implications for Trace Metal Speciation. *Geochim. Cosmochim. Acta* **2002**, *66* (18), 3211–3224. https://doi.org/10.1016/S0016-7037(02)00930-4.

(10) Aiken, G. R.; Hsu-Kim, H.; Ryan, J. N. Influence of Dissolved Organic Matter on the Environmental Fate of Metals, Nanoparticles, and Colloids. *Environ. Sci. Technol.* **2011**, *45* (8), 3196–3201. https://doi.org/10.1021/es103992s.

(11) Guénet, H.; Davranche, M.; Vantelon, D.; Gigault, J.; Prévost, S.; Taché, O.; Jaksch, S.; Pédrot, M.; Dorcet, V.; Boutier, A.; Jestin, J. Characterization of Iron–Organic Matter Nano-Aggregate Networks through a Combination of SAXS/SANS and XAS Analyses: Impact on As Binding. *Environ. Sci. Nano* **2017**, *4* (4), 938–954. https://doi.org/10.1039/C6EN00589F.

(12) Pradel, A.; Ferreres, S.; Veclin, C.; El Hadri, H.; Gautier, M.; Grassl, B.; Gigault, J. Stabilization of Fragmental Polystyrene Nanoplastic by Natural Organic Matter: Insight into Mechanisms. *ACS EST Water* **2021**, *1* (5), 1198–1208. https://doi.org/10.1021/acsestwater.0c00283.

(13) Vindedahl, A. M.; Strehlau, J. H.; Arnold, W. A.; Penn, R. L. Organic Matter and Iron Oxide Nanoparticles: Aggregation, Interactions, and Reactivity. *Environ. Sci. Nano* **2016**, *3* (3), 494–505. https://doi.org/10.1039/C5EN00215J.

(14) Cheng, W.; Zhou, L.; Marsac, R.; Boily, J.-F.; Hanna, K. Effects of Organic Matter–Goethite Interactions on Reactive Transport of Nalidixic Acid: Column Study and Modeling. *Environ. Res.* **2020**, *191*, 110187. https://doi.org/10.1016/j.envres.2020.110187.

(15) Kleber, M.; Bourg, I. C.; Coward, E. K.; Hansel, C. M.; Myneni, S. C. B.; Nunan, N. Dynamic Interactions at the Mineral–Organic Matter Interface. *Nat. Rev. Earth Environ.* **2021**, *2* (6), 402–421. https://doi.org/10.1038/s43017-021-00162-y.

(16) Kleber, M.; Sollins, P.; Sutton, R. A Conceptual Model of Organo-Mineral Interactions in Soils: Self-Assembly of Organic Molecular Fragments into Zonal Structures on Mineral Surfaces. *Biogeochemistry* **2007**, *85* (1), 9–24. https://doi.org/10.1007/s10533-007-9103-5.

(17) Lehmann, J.; Kleber, M. The Contentious Nature of Soil Organic Matter. *Nature* **2015**, *528* (7580), 60–68. https://doi.org/10.1038/nature16069.
(18) Reiller, P. E. Modelling Metal–Humic Substances–Surface Systems: Reasons for Success, Failure and Possible Routes for Peace of Mind. *Mineral. Mag.* **2012**, *76* (7), 2643–2658. https://doi.org/10.1180/minmag.2012.076.7.02.
(19) Weng, L.; Van Riemsdijk, W. H.; Hiemstra, T. Effects of Fulvic and Humic Acids on Arsenate Adsorption to Goethite: Experiments and Modeling. *Environ. Sci. Technol.* **2009**, *43* (19), 7198–7204. https://doi.org/10.1021/es9000196.
(20) Buffle, J. Complexation Reactions in Aquatic Systems; Analytical Approach. *Acta Hydrochim. Hydrobiol.* **1989**, *17* (2), 230–230. https://doi.org/10.1002/aheh.19890170220.
(21) Christensen, J. B.; Tipping, E.; Kinniburgh, D. G.; Grøn, C.; Christensen, T. H. Proton Binding by Groundwater Fulvic Acids of Different Age, Origins, and Structure Modeled with the Model V and NICA−Donnan Model. *Environ. Sci. Technol.* **1998**, *32* (21), 3346–3355. https://doi.org/10.1021/es971134o.
(22) Gustafsson, J. P. Modeling the Acid–Base Properties and Metal Complexation of Humic Substances with the Stockholm Humic Model. *J. Colloid Interface Sci.* **2001**, *244* (1), 102–112. https://doi.org/10.1006/jcis.2001.7871.
(23) Kinniburgh, D. G.; van Riemsdijk, W. H.; Koopal, L. K.; Borkovec, M.; Benedetti, M. F.; Avena, M. J. Ion Binding to Natural Organic Matter: Competition, Heterogeneity, Stoichiometry and Thermodynamic Consistency. *Colloids Surf. Physicochem. Eng. Asp.* **1999**, *151* (1–2), 147–166. https://doi.org/10.1016/S0927-7757(98)00637-2.
(24) Ritchie, J. D.; Perdue, E. M. Proton-Binding Study of Standard and Reference Fulvic Acids, Humic Acids, and Natural Organic Matter. *Geochim. Cosmochim. Acta* **2003**, *67* (1), 85–96. https://doi.org/10.1016/S0016-7037(02)01044-X.
(25) Tipping, E. Humic Ion-Binding Model VI: An Improved Description of the Interactions of Protons and Metal Ions with Humic Substances. *Aquat. Geochem.* **1998**, *4* (1), 3–47. https://doi.org/10.1023/A:1009627214459.
(26) Koopal, L. K.; Saito, T.; Pinheiro, J. P.; Riemsdijk, W. H. van. Ion Binding to Natural Organic Matter: General Considerations and the NICA–Donnan Model. *Colloids Surf. Physicochem. Eng. Asp.* **2005**, *265* (1–3), 40–54. https://doi.org/10.1016/j.colsurfa.2004.11.050.
(27) Milne, C. J.; Kinniburgh, D. G.; Tipping, E. Generic NICA-Donnan Model Parameters for Proton Binding by Humic Substances. *Environ. Sci. Technol.* **2001**, *35* (10), 2049–2059. https://doi.org/10.1021/es000123j.
(28) Gustafsson, J. P.; Persson, I.; Kleja, D. B.; Van Schaik, J. W. J. Binding of Iron(III) to Organic Soils: EXAFS Spectroscopy and Chemical Equilibrium Modeling. *Environ. Sci. Technol.* **2007**, *41* (4), 1232–1237. https://doi.org/10.1021/es0615730.
(29) Marsac, R.; Catrouillet, C.; Davranche, M.; Bouhnik-Le Coz, M.; Briant, N.; Janot, N.; Otero-Fariña, A.; Groenenberg, J. E.; Pédrot, M.; Dia, A. Modeling Rare Earth Elements Binding to Humic Acids with Model VII. *Chem. Geol.* **2021**, *567*, 120099. https://doi.org/10.1016/j.chemgeo.2021.120099.
(30) Neweshy, W.; Planas, D.; Tellier, E.; Demers, M.; Marsac, R.; Couture, R.-M. Response of Sediment Phosphorus Partitioning to Lanthanum-Modified Clay Amendment and Porewater Chemistry in a Small Eutrophic Lake. *Environ. Sci. Process. Impacts* **2022**. https://doi.org/10.1039/D1EM00544H.
(31) Dryer, D. J.; Korshin, G. V.; Fabbricino, M. In Situ Examination of the Protonation Behavior of Fulvic Acids Using Differential Absorbance Spectroscopy. *Environ. Sci. Technol.* **2008**, *42* (17), 6644–6649. https://doi.org/10.1021/es800741u.
(32) Janot, N.; Reiller, P. E.; Korshin, G. V.; Benedetti, M. F. Using Spectrophotometric Titrations To Characterize Humic Acid Reactivity at Environmental Concentrations. *Environ. Sci. Technol.* **2010**, *44* (17), 6782–6788. https://doi.org/10.1021/es1012142.
(33) Liu, S.; Benedetti, M. F.; Han, W.; Korshin, G. V. Comparison of the Properties of Standard Soil and Aquatic Fulvic and Humic Acids Based on the Data of Differential Absorbance and Fluorescence Spectroscopy. *Chemosphere* **2020**, *261*, 128189. https://doi.org/10.1016/j.chemosphere.2020.128189.

(34) Tesfa, M.; Dia, A.; Ollivier, M.; Osorio-Leon, I.-D.; Marsac, R. An Easy Spectrophotometric Acid-Base Titration Protocol for Dissolved Organic Matter. *MethodsX* **2022**, *9*, 101721. https://doi.org/10.1016/j.mex.2022.101721.
(35) Yan, M.; Dryer, D.; Korshin, G. V. Spectroscopic Characterization of Changes of DOM Deprotonation–Protonation Properties in Water Treatment Processes. *Chemosphere* **2016**, *148*, 426–435. https://doi.org/10.1016/j.chemosphere.2016.01.055.
(36) Conte, P.; Piccolo, A. Conformational Arrangement of Dissolved Humic Substances. Influence of Solution Composition on Association of Humic Molecules. *Environ. Sci. Technol.* **1999**, *33* (10), 1682–1690. https://doi.org/10.1021/es9808604.
(37) Korshin, G. V.; Li, C.-W.; Benjamin, M. M. Monitoring the Properties of Natural Organic Matter through UV Spectroscopy: A Consistent Theory. *Water Res.* **1997**, *31* (7), 1787–1795. https://doi.org/10.1016/S0043-1354(97)00006-7.
(38) Yan, M.; Korshin, G. V.; Claret, F.; Croué, J.-P.; Fabbricino, M.; Gallard, H.; Schäfer, T.; Benedetti, M. F. Effects of Charging on the Chromophores of Dissolved Organic Matter from the Rio Negro Basin. *Water Res.* **2014**, *59*, 154–164. https://doi.org/10.1016/j.watres.2014.03.044.
(39) Janot, N.; Reiller, P. E.; Zheng, X.; Croué, J.-P.; Benedetti, M. F. Characterization of Humic Acid Reactivity Modifications Due to Adsorption onto α-Al2O3. *Water Res.* **2012**, *46* (3), 731–740. https://doi.org/10.1016/j.watres.2011.11.042.
(40) Tesfa, M.; Duval, J. F. L.; Marsac, R.; Dia, A.; Pinheiro, J.-P. Absolute and Relative Positioning of Natural Organic Matter Acid–Base Potentiometric Titration Curves: Implications for the Evaluation of the Density of Charged Reactive Sites. *Environ. Sci. Technol.* **2022**, acs.est.2c00828. https://doi.org/10.1021/acs.est.2c00828.
(41) Cincotta, M. M.; Perdrial, J. N.; Shavitz, A.; Libenson, A.; Landsman-Gerjoi, M.; Perdrial, N.; Armfield, J.; Adler, T.; Shanley, J. B. Soil Aggregates as a Source of Dissolved Organic Carbon to Streams: An Experimental Study on the Effect of Solution Chemistry on Water Extractable Carbon. *Front. Environ. Sci.* **2019**, *7*, 172. https://doi.org/10.3389/fenvs.2019.00172.
(42) Fernandes, A. N.; Giacomelli, C.; Giovanela, M.; Vaz, D. O.; Szpoganicz, B.; Sierra, M. M. D. Potentiometric Acidity Determination in Humic Substances Influenced by Different Analytical Procedures. *J. Braz. Chem. Soc.* **2009**, *20* (9), 1715–1723. https://doi.org/10.1590/S0103-50532009000900021.
(43) Ritchie, J. D.; Perdue, E. M. Analytical Constraints on Acidic Functional Groups in Humic Substances. *Org. Geochem.* **2008**, *39* (6), 783–799. https://doi.org/10.1016/j.orggeochem.2008.03.003.
(44) Rodríguez, F. J.; Schlenger, P.; García-Valverde, M. Monitoring Changes in the Structure and Properties of Humic Substances Following Ozonation Using UV–Vis, FTIR and 1H NMR Techniques. *Sci. Total Environ.* **2016**, *541*, 623–637. https://doi.org/10.1016/j.scitotenv.2015.09.127.
(45) Guggenberger, G.; Zech, W.; Haumaier, L.; Christensen, B. T. Land-Use Effects on the Composition of Organic Matter in Particle-Size Separates of Soils: II. CPMAS and Solution 13C NMR Analysis. *Eur. J. Soil Sci.* **1995**, *46* (1), 147–158. https://doi.org/10.1111/j.1365-2389.1995.tb01821.x.
(46) Machado, W.; Franchini, J. C.; de Fátima Guimarães, M.; Filho, J. T. Spectroscopic Characterization of Humic and Fulvic Acids in Soil Aggregates, Brazil. *Heliyon* **2020**, *6* (6), e04078. https://doi.org/10.1016/j.heliyon.2020.e04078.
(47) Yan, M.; Wang, D.; Korshin, G. V.; Benedetti, M. F. Quantifying Metal Ions Binding onto Dissolved Organic Matter Using Log-Transformed Absorbance Spectra. *Water Res.* **2013**, *47* (7), 2603–2611. https://doi.org/10.1016/j.watres.2013.02.044.